Applied Physics Letters

RESEARCH ARTICLE | JUNE 27 2023

Ablation loading of barium ions into a surface-electrode trap

X. Shi ; S. L Todaro ; G. L. Mintzer ; C. D. Bruzewicz ; J. Chiaverini ; I. L. Chuang

Appl. Phys. Lett. 122, 264002 (2023)
https://doi.org/10.1063/5.0149778
CHORUS

AIP Publishing

Applied Physics Letters ARTICLE pubs.aip.org/aip/apl

Ablation loading of barium ions into a surface-electrode trap

Cite as: Appl. Phys. Lett. **122**, 264002 (2023); doi: 10.1063/5.0149778
Submitted: 8 March 2023 · Accepted: 6 June 2023 ·
Published Online: 27 June 2023

X. Shi,[1] S. L Todaro,[1,a)] G. L. Mintzer,[1] C. D. Bruzewicz,[2,3] J. Chiaverini,[2,3] and I. L. Chuang[1]

AFFILIATIONS

[1]Center for Ultracold Atoms, Research Laboratory of Electronics, Massachusetts Institute of Technology, Cambridge, Massachusetts 02139, USA
[2]Lincoln Laboratory, Massachusetts Institute of Technology, Lexington, Massachusetts 02421, USA
[3]Center for Quantum Engineering, Research Laboratory of Electronics, Massachusetts Institute of Technology, Cambridge, Massachusetts 02139, USA

[a)]**Author to whom correspondence should be addressed:** stodaro@mit.edu

ABSTRACT

Trapped-ion quantum information processing may benefit from qubits encoded in isotopes that are practically available in only small quantities, e.g., due to low natural abundance or radioactivity. Laser ablation provides a method of controllably liberating neutral atoms or ions from low-volume targets, but energetic ablation products can be difficult to confine in the small ion-electrode distance, micron-scale microfabricated traps amenable to high-speed, high-fidelity manipulation of ion arrays. Here, we investigate ablation-based ion loading into surface-electrode traps of different sizes to test a model describing ion loading probability as a function of effective trap volume and other trap parameters. We characterize loading of ablated barium from a metallic source in two cryogenic surface-electrode traps with 730 and 50 μm ion-electrode distances. Our loading rate agrees with a predictive analytical model, providing insight for the confinement of limited-quantity species of interest for quantum computing, simulation, and sensing.

Singly ionized barium has recently emerged as a leading ion species for trapped-ion quantum information processing, with a low-lying level structure controllable by visible and near-infrared lasers and a long-lived $^2D_{5/2}$ metastable state with a radiative decay lifetime of more than 30 seconds.[1] Additionally, since relevant laser wavelengths for manipulation of Ba^+ are, in general, longer than those for most comparable ion species, integration of control technologies may be simplified. Particular attention has been paid to the radioactive isotope $^{133}Ba^+$, which has nuclear spin $I = 1/2$ (Refs. 2–4). Due to its low, non-zero nuclear spin, this isotope has "clock" transitions between hyperfine sublevels of both the ground and metastable states that are first-order insensitive to magnetic field fluctuations[5] with a minimally complex electronic structure. This favorable electronic structure has enabled fast fiducial electronic state preparation with low state preparation and measurement error.[3] However, $^{133}Ba^+$ has a half life of 10.5 years, so safe use suggests employing very small (microgram) quantities to avoid contamination or the requirement for excessive shielding. Ions of nonradioactive Ba isotopes are often loaded via an oven, from which atoms in a vapor are ionized within the trap region by means of electron-beam bombardment[6] or photoionization[7–9] (PI). Standard ovens are inefficient, however, producing uncollimated atomic beams and generally coating the apparatus in excess source material and so are not ideal for a radioactive source.

Alternatively, either neutral or ionized atoms can be generated by laser ablation of a source target,[10–13] which produces a directed plume of material. Ablation results in less excess material deposition and introduces a smaller heat load to the apparatus when compared to use of an oven, a benefit for cryogenic or portable system operation. Initial demonstrations of trapping and coherent control of $^{133}Ba^+$ were based on direct ionization via ablation of radioactive $BaCl_2$.[2,3] Photoionization of ablated neutral barium atoms and subsequent ion trapping from a small volume target compatible with a radioactive source has also been demonstrated,[4] further advancing the promise of $BaCl_2$ sources for quantum computing applications. However, these demonstrations of trapping ablated barium were performed in relatively large, three-dimensional radio frequency (rf) Paul traps.[4,14] Surface-electrode traps[15] are a desirable alternative for scaling ion-based quantum computers, as they can utilize modern microfabrication processes[16] and introduce the opportunity to miniaturize and integrate technologies such as control electronics,[17]

laser light delivery,[18–20] and single-photon detectors[21–23] on-chip. However, surface traps have saddle (escape) points at relatively low potential energies compared to 3D Paul traps of similar size and rf drive parameters,[15] making it more challenging to contain highly energetic ions. Furthermore, rf breakdown in microfabricated traps can limit the ultimate achievable depth.[24] Loading low-abundance or radioactive species into surface traps, therefore, requires specialized techniques.

Here, we describe loading of $^{138}Ba^+$ ions, via laser ablation, into segmented linear surface-electrode traps in a cryogenic vacuum system. We characterize the efficiency of ion loading via photoionization of neutral atoms in the ablation plume from a pure barium target. Using both strontium loaded from a pre-cooled source and barium ions ablated from this metallic target, we analyze ion loading into two-surface-electrode-trap designs of very different sizes; the results are used to validate a model proposed to allow prediction of relative loading efficiency as a function of rf-trap parameters. We additionally demonstrate loading ions from ablation using a variety of compound barium sources, some amenable to radioactive source preparation. The described model and loading methodologies are generally applicable to quantum information processing with registers of rare ionic species, including $^{133}Ba^+$, in microfabricated surface-electrode traps.

The experiments are conducted in a standard cryogenic ion-trapping system, documented previously;[25–28] here, we describe aspects that are particular to this work. Barium ions are loaded through laser ablation followed by photoionization, and strontium ions are photoionized from a remote, pre-cooled neutral source.[25,27] The ablation loading setup is shown in Fig. 1(a). We use a Q-switched Nd:YAG pulsed laser (Continuum Minilite II) operated in its fundamental mode at 1064 nm with a pulse duration of 5–7 ns. The beam is focused down to a waist radius of 100 μm at the target location with a fluence of 1 J cm^{-2}. The ablation laser propagates along the axial direction of the trap [the y axis as shown in Fig. 1(a)] and is tilted at an angle in the yz plane to avoid scattering on the trap surface. Neutral barium atoms produced by ablation are subsequently ionized through a two-step photoionization process,[9] using 554 and 405 nm lasers, oriented as shown in Fig. 1(a). The 554 nm laser beam is oriented perpendicularly to the plume generated by ablation to minimize Doppler shifts. All other lasers (for Sr^+ photoionization, Doppler cooling, and repumping; and for Ba^+ Doppler cooling and repumping) are overlapped at the ion location, making a 45° angle with respect to the trap axis. Scattered photons are imaged, using a dual-wavelength high-NA lens (optimized for 422 and 493 nm, the wavelengths of the Sr^+ and Ba^+ detection transitions, respectively) onto either a photo-multiplier tube (PMT) or an electron-multiplying charge-coupled-device (EMCCD) camera.

Several ablation target materials and production methods were investigated (see the supplementary material); a metallic target was used for the loading efficiency measurements presented here. This target is barium metal (dendritic, 99.8% purity), prepared by compressing a single piece to form a rectangular prism, approximately $10 \times 3 \times 1$ mm^3 in size, mounted 11.4 mm away from the trap center [cf. Fig. 1(a)]. The metallic target typically obtains a layer of barium oxide during approximately 5 min of exposure to air required for installation. This oxide layer is then ablated with 5–10 pulses at a high ablation-beam fluence (5–7 J cm^{-2}), while neutral barium fluorescence at 554 nm is monitored using the PMT until sufficient flux is observed.

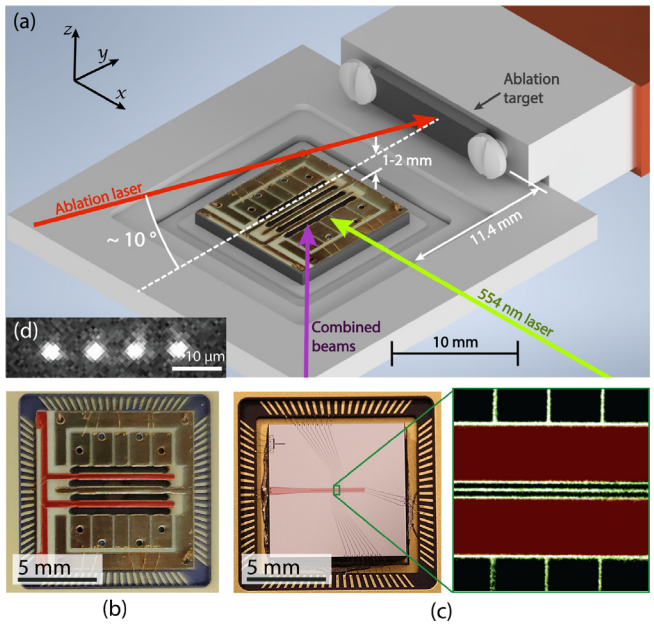

FIG. 1. Traps and experimental configuration. (a) Beam orientations and trap mounting hardware. (b) and (c) The printed-circuit-board and microfabricated surface electrode traps. The electrodes at the top and bottom of the detail image of the microfabricated trap are segmented with a pitch of 120 μm. The rf drive is applied to the electrode shown in red in both systems (false color). Ions are trapped (b) 730 and (c) 50 μm above the trap surface. Traps are mounted in ceramic pin grid array (CPGA) mounts for rapid trap exchange. (d) Four Ba^+ ions in the microfabricated trap.

A black spot can usually be seen on the target afterward, and ions are loaded from neutral atoms produced by ablating this spot at the lower (standard) fluence of 1 J cm^{-2}. While an increased loading rate per pulse can be achieved at higher fluence, we also observe a concomitant increase in the rate of contamination of the trap with particles that can scatter control laser beams or become charged by liberated electrons. We, therefore, combine low fluence pulses with a higher repetition rate (10–15 Hz) for rapid loading and minimal contamination.

Two traps were used in this work. The first is a linear printed-circuit board surface-electrode Paul trap (the PCB trap, also known as Bastille[10,29,30]), and the second is a sputtered-Nb-on-sapphire microfabricated linear Paul trap[25,31] [the microfabricated trap; see Figs. 1(b) and 1(c) for images of both traps]. In the PCB trap, the ion height is 730 μm, and the rf drive at a frequency of 7.1 MHz was used, with Ba^+ secular frequencies of 165–295 kHz radial and approximately 100 kHz axial. For the microfabricated trap, the ion height is 50 μm, and the rf frequency was 41.1 MHz, with Ba^+ secular frequencies of 1.9–3.3 MHz radial and 500–600 kHz axial.

We model the ion loading probability in both traps by first determining the relevant trap volume in which photoionized atoms would nominally be confined indefinitely, neglecting heating effects but including effects of rf excitation (micromotion). We, however, neglect laser cooling since trap dynamics are expected to be much faster than typical Doppler cooling timescales, particularly for ions created near the edge of the effective trap volume. We calculate the trap potential using an analytic model of the surface-electrode trap geometry[32] (see the supplementary material for details). For the trapping potential

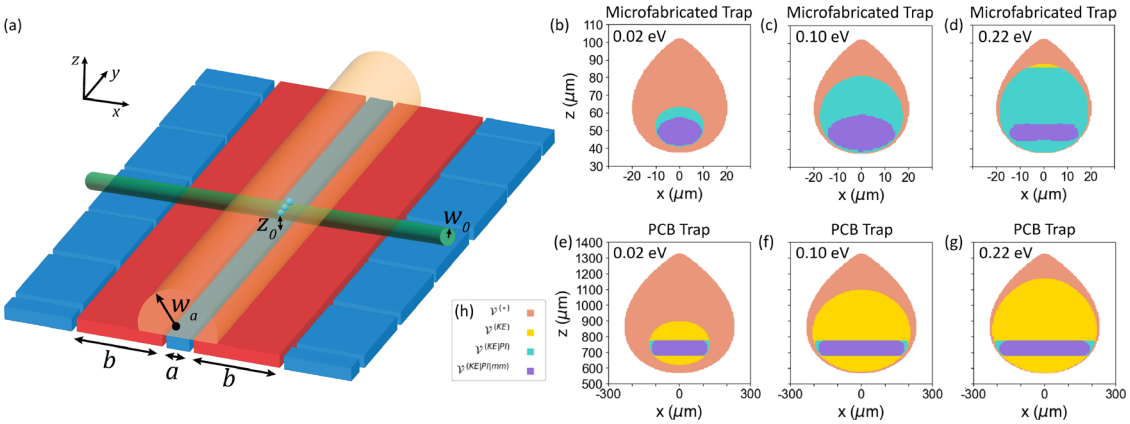

FIG. 2. Experimental geometry and relevant trap volumes. (a) The trap geometry we consider. The trap rf null is aligned with the y axis. The drive rf, with amplitude V_{rf} and angular frequency Ω_{rf}, is applied to the two electrodes shown in red, of width b and separated by a distance a. The electrodes shown in blue allow the creation of a DC trapping potential. We assume neutral atom flux (orange) of uniform density and radius w_a, aligned with the y axis. The photoionization beams (green) with radius w_0 are delivered perpendicularly to the atom flux. Ions (not to scale) are trapped a distance z_0 above the electrodes. (b)–(d) Cross sections of trap volumes in the microfabricated trap as a function of increasing V_{rf}, from left to right, for an incoming Ba atom moving at $v = 150\,\mathrm{ms}^{-1}$. (e)–(g) Similar cross sections of trap volumes in the PCB trap. Trap depths E_{max} are notated for all cross sections (b)–(g). For all cross sections, the colors are as indicated in inset (h): the bare trapping volume $\mathcal{V}^{(\circ)}$ is shown in pink, the kinetic energy truncated trapping volume $\mathcal{V}^{(\mathrm{KE})}$ in yellow, the PI-intersected trapping volume $\mathcal{V}^{(\mathrm{KE|PI})}$ in teal, and the micromotion-corrected stable trapping volume $\mathcal{V}^{(\mathrm{KE|PI|mm})}$ in purple. Note that these are overlapping volumes.

we investigate, the potential varies slowly and negligibly in the axial direction within the section of the trapping region defined by the PI beams [cf. Fig. 2(a)], so we compare 2D slices of the volumes in the radial xz plane.

As illustrated in Fig. 2, the bare stable trapping volume $\mathcal{V}^{(\circ)}$ is the region for which the potential energy (characterized by the pseudopotential $\phi_{rf}(\vec{x})$ and the residual DC potential $\phi_{DC}(\vec{x})$) of an ion created at a particular location $\vec{x}$ is less than the potential energy at the trap escape point E_{max} (the trap depth). In our simulations, to update $\mathcal{V}^{(\circ)}$ considering ions with non-zero velocity, we assume that an atom of kinetic energy KE is trapped if and only if $\phi_{DC}(\vec{x}) + \phi_{rf}(\vec{x}) + KE \leq E_{max}$; otherwise, the ion will escape within a few trap cycles. The region defined by this effective trap depth $E_{max} - KE$ defines the (velocity dependent) kinetic-energy truncated trapping volume $\mathcal{V}^{(\mathrm{KE})}$. The trap volume also depends on the region of sufficient PI beam intensities, since we consider only ions produced within the trapping region. We define the photoionized trapping volume $\mathcal{V}^{(\mathrm{KE|PI})}$ as the intersection of $\mathcal{V}^{(\mathrm{KE})}$ with the $1/e^2$ radius of the PI beams.

For ions generated far from the trap center, the trap dynamics must also be considered, and $\mathcal{V}^{(\mathrm{KE|PI})}$ is further reduced by effects due to micromotion. We, therefore, investigate approximate solutions to the Mathieu equations[33,34] to determine ion trajectories for starting positions $\vec{x}$ within $\mathcal{V}^{(\mathrm{KE|PI})}$. If the ion leaves $\mathcal{V}^{(\mathrm{KE})}$ within a single secular period, we reject the starting point from the rf-dynamics-limited volume $\mathcal{V}^{(\mathrm{KE|PI|mm})}$; the remaining points constitute this volume.

From this volume determination and known behavior of the ablation and photoionization processes, we calculate the probability of trapping, up to an overall scale factor, by integrating over atom velocity v,

$$P_{trap} \propto \frac{I_2 w_0}{w_a^2 k_B T} \int_0^{v_{max}} \mathcal{V}^{(\mathrm{KE|PI|mm})} \left(\frac{1 - e^{-\gamma_1 w_0/2v}}{v}\right) \times e^{-m(v-v_0)^2/2k_B T}\, dv. \quad (1)$$

Here, m is the atomic mass, $v_{max} \equiv \sqrt{2E_{max}/m}$ is the velocity corresponding to a kinetic energy equal to the trap depth E_{max}, v_0 is the center-of-mass velocity of the ablation plume, k_B is Boltzmann's constant, T is the temperature of the ablation plume, w_a is the radius of the ablation plume, w_0 is the radius of the focused photoionization lasers, γ_1 is the saturated first-stage PI linewidth, and I_2 is the intensity of the second-stage PI laser. The derivation of Eq. (1) is discussed in detail in the supplementary material.

We validate this theoretical model by measuring the relative probability of trapping an ion in both traps as a function of rf drive amplitude. To compare traps with very different driving conditions (due to differing ion-electrode distances and rf frequencies), we utilize the trap depth. The trap depth due to rf confinement generally depends on both rf amplitude V_{rf} and drive frequency Ω_{rf} by

$$E_{max}^{(rf)} = \frac{q^2 V_{rf}^2}{\pi^2 m \Omega_{rf}^2 z_0^2} \kappa(a, b), \quad (2)$$

where q is the ion charge, m is the ion mass, z_0 is the ion-electrode distance, and $\kappa(a, b)$ is a dimensionless factor dependent on trap geometry parameters a and b (Ref. 35 and supplementary material). The trap depth is reduced by the application of DC trapping voltages. We distinguish between the "rf trap depth" (the trap depth in the absence of the DC potential) and the true trap depth and describe both in the supplementary material. We report here loading rates as a function of rf trap depth. We extract both the axial trap frequency and the rf amplitude (and thus the trap depth) from secular frequency measurements using standard techniques.[36,37]

Loading rate is defined as the number of ions loaded per attempt. A single Ba^+ loading attempt is made using one pulse of the ablation laser, while a single Sr^+ attempt is made by unblocking a beam that delivers neutral Sr from the pre-cooled source for 1 s. Therefore, absolute numbers of Ba^+ and Sr^+ loaded should not be compared.

Ion presence is confirmed by collecting scattered photons (at 493 or 422 nm) for 10 ms, with the optimal Poissonian discrimination threshold calibrated using a single, Doppler-cooled ion.[38] For Ba^+ loading in both traps and Sr^+ loading in the microfabricated trap, we loaded either zero or one ion per attempt. In these cases, we calculated the loading rate by counting trials in which the scattered photon counts exceeded the discrimination threshold. By contrast, in the PCB trap, we regularly loaded multiple Sr^+ ions for parameters that led to single ion loading in the other cases. Therefore, we calculated the loading rate of Sr^+ in the PCB trap by estimating the number of ions loaded per trial: we divide the total number of photons by the average number of bright photons for a single ion. We eject ions after each trial by turning off the rf drive.

Results from these measurements, along with fits to the model (the single-fit parameter being an overall scale factor), are shown in Fig. 3. Both statistical error in the measured loading rates and estimated errors in the model due to parameter uncertainties are shown; the latter is discussed in detail in the supplementary material. At low rf trap depths, the probability of trapping sharply increases with increasing trap depth after a threshold rf amplitude V_{th} (corresponding to threshold rf trap depth ϕ_{th}) determined by total potential positivity (see the supplementary material). At higher trap depths, loading efficiency in the microfabricated trap drops with increasing trap depth. This behavior is due to reduction of the stable trapping volume $\mathcal{V}^{(\mathrm{KE|PI|mm})}$ at high amplitudes arising from Paul trap instability (see the supplementary material). This leads to optimal trapping conditions at an rf trap depth of

$$E_{\mathrm{opt}}^{(rf)} \approx \frac{1}{2} m \left(v_0 + \sqrt{\frac{k_{\mathrm{B}} T}{m}} \right)^2 + \phi_{\mathrm{th}}, \tag{3}$$

which is approximately 0.10 eV for ablated barium, as detailed in the supplementary material. The experimentally observed reduction is qualitatively consistent with predictions from the theoretical model. At the upper end of attainable trap depths in the microfabricated trap, the micromotion amplitude is large throughout a substantial fraction of $\mathcal{V}^{(\mathrm{KE|PI})}$, reducing $\mathcal{V}^{(\mathrm{KE|PI|mm})}$. We observed no reduction of the loading rate in the PCB trap with increasing trap depths for the rf amplitudes achievable in our apparatus. This is consistent with the model's predictions, since the micromotion amplitude remains small over a similar fraction of $\mathcal{V}^{(\mathrm{KE|PI})}$ in the physically larger PCB trap over this range. However, we note that due to experimental limitations, we were unable to explore the same range of trap depths in the PCB trap as the microfabricated trap. We observe a somewhat faster reduction in loading rate at high trap depths in the microfabricated trap than is predicted, suggesting that there is some behavior in this regime that is not fully accounted for in the model.

We observe a higher loading rate for the larger PCB trap than for the microfabricated trap at all trap depths, despite the higher trap depth attainable in the significantly smaller microfabricated trap. This is attributable to the larger trapping volume in the PCB trap, in which $\mathcal{V}^{(\mathrm{KE|PI})}$ is approximately a factor of 150 larger, owing to its physically larger dimensions.

For this demonstration, we loaded ions from an ablated barium metal source. This is incompatible with trapping the isotope $^{133}Ba^+$, as radioactively enhanced pure Ba metal is not readily available. Ablation of $BaCl_2$, a viable source for $^{133}Ba^+$ atoms, was previously shown to produce neutral Ba with an average temperature of $T = 37\,000$ K,[4]

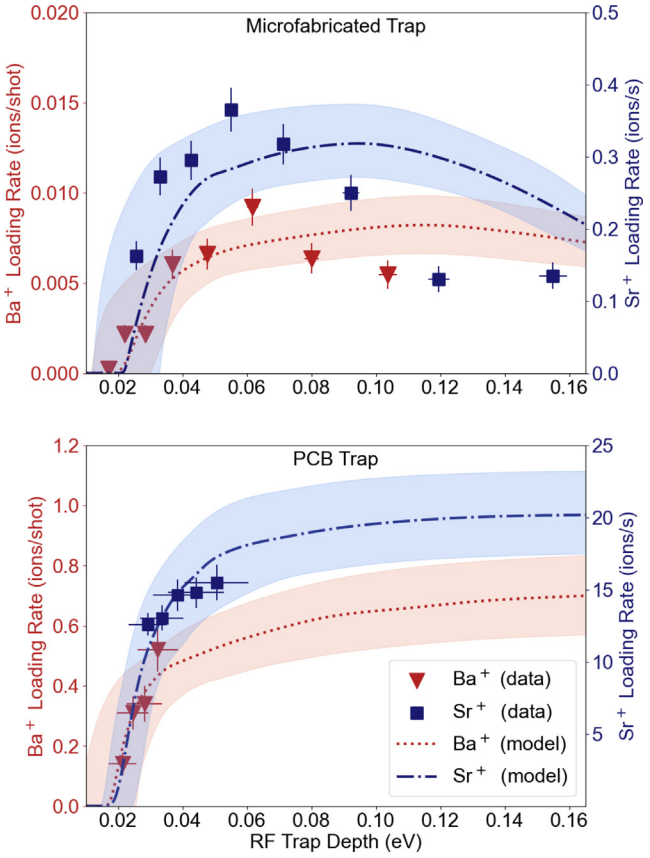

FIG. 3. Loading rate vs rf trap depth. Measurements for Ba^+ (red triangles, left axis with red labels) and Sr^+ (blue squares, right axis with blue labels), for both the microfabricated (top) and the PCB (bottom) traps. Barium loading rates are in units of ions loaded per ablation pulse (shot), while strontium loading rates are in units of ions loaded per second from a continuous pre-cooled source, as described in the text. Error bars represent one standard deviation. Dashed lines are single-parameter fits to the model, and the shaded regions incorporate uncertainties in the model due to fluctuations in beam pointing, PI intensity, atomic velocity distributions, shot-to-shot variability in target efficiency, and stray electric field. We smooth discrete jumps in the model values due to finite-step size of the numerical integration using a cubic spline fit. The analytically calculated threshold rf trap depth is $\phi_{\mathrm{th}} \sim 0.02$ eV, and the peak loading rate trap depth is $E_{\mathrm{opt}}^{(rf)} \sim 0.08 + \phi_{\mathrm{th}} = 0.10$ eV for Ba^+ in the microfabricated trap, consistent with the data.

more than an order of magnitude higher than the melting point of Ba metal. We loaded ions from $BaCl_2$-based targets into both traps (described in the supplementary material), but the loading rates and target lifetimes were sufficiently small as to preclude quantitative analysis. We attribute this behavior to the higher temperature of liberated atoms, for which our model predicts a reduction by roughly an order of magnitude in loading probability. This presents a challenge when loading microfabricated traps from low-volume radioactive sources. On the other hand, the results presented here suggest that an *in situ* chemical reaction in which a more reactive metal is allowed to bond with the chlorine, leaving free barium, could dramatically improve the probability of loading Ba^+ from ablation of a $BaCl_2$ source (after such preparation). In fact, we were able to load Ba^+ ions using this method (see the

supplementary material), but more work must be done to fully characterize the loading efficiency.

The model also has implications for the design of future trapped-ion systems, as there is interest in continued miniaturization of microfabrication-compatible traps to address speed and scaling challenges in quantum information processing. The relative loading rates observed between the PCB and microfabricated traps as well as the model describing their performance confirm that loading rates drop as the trap volume is reduced, highlighting the difficulties of loading rare species into increasingly miniaturized traps, regardless of trap depth. We suggest the consideration of the stable trapping volume as described here as an additional valuable metric in trap design. For instance, small loading rates in low-volume traps could be compensated through the inclusion of a high-volume loading zone and a transition region.

See the supplementary material for details of the ablation target, derivation of the theoretical loading model, derivation of threshold and optimal loading trap depths, and discussion of model parameters and errors.

This research was supported by the U.S. Army Research Office through Grant No. W911NF-20-1-0037 and by the NSF Center for Ultracold Atoms. S.L.T. is supported by an appointment to the Intelligence Community Postdoctoral Research Fellowship Program at MIT, administered by Oak Ridge Institute for Science and Education through an interagency agreement between the U.S. Department of Energy and the Office of the Director of National Intelligence. The authors thank Andrew Jayich, Eric Hudson, and Wes Campbell and their research groups for helpful discussions.

AUTHOR DECLARATIONS

Conflict of Interest

The authors have no conflicts to disclose.

Author Contributions

Xiaoyang Shi and Susanna L. Todaro contributed equally to this work.

Xiaoyang Shi: Conceptualization (equal); Formal analysis (equal); Investigation (equal); Methodology (equal); Resources (equal); Software (equal); Validation (equal); Visualization (equal); Writing – original draft (equal); Writing – review & editing (equal). **Susanna L. Todaro:** Conceptualization (equal); Formal analysis (equal); Investigation (equal); Methodology (equal); Software (equal); Validation (equal); Visualization (equal); Writing – original draft (equal); Writing – review & editing (equal). **Gabriel L. Mintzer:** Software (equal); Writing – review & editing (equal). **Colin D. Bruzewicz:** Methodology (equal); Supervision (equal); Writing – review & editing (equal). **John Chiaverini:** Conceptualization (equal); Funding acquisition (equal); Methodology (equal); Project administration (equal); Supervision (equal); Writing – review & editing (equal). **Isaac L. Chuang:** Conceptualization (equal); Funding acquisition (equal); Methodology (equal); Project administration (equal); Writing – review & editing (equal).

DATA AVAILABILITY

The data that support the findings of this study are available from the corresponding author upon reasonable request.

REFERENCES

[1]C. Auchter, T. W. Noel, M. R. Hoffman, S. R. Williams, and B. B. Blinov, "Measurement of the branching fractions and lifetime of the $5D_{5/2}$ level of Ba^+," Phys. Rev. A **90**, 060501 (2014).
[2]D. Hucul, J. E. Christensen, E. R. Hudson, and W. C. Campbell, "Spectroscopy of a synthetic trapped ion qubit," Phys. Rev. Lett. **119**, 100501 (2017).
[3]J. E. Christensen, D. Hucul, W. C. Campbell, and E. R. Hudson, "High-fidelity manipulation of a qubit enabled by a manufactured nucleus," npj Quantum Inf. **6**, 35 (2020).
[4]B. M. White, P. J. Low, Y. de Sereville, M. L. Day, N. Greenberg, R. Rademacher, and C. Senko, "Isotope-selective laser ablation ion-trap loading of $^{137}Ba^+$ using a $BaCl_2$ target," Phys. Rev. A **105**, 033102 (2022).
[5]C. Langer, R. Ozeri, J. D. Jost, J. Chiaverini, B. DeMarco, A. Ben-Kish, R. B. Blakestad, J. Britton, D. B. Hume, W. M. Itano, D. Leibfried, R. Reichle, T. Rosenband, T. Schaetz, P. O. Schmidt, and D. J. Wineland, "Long-lived qubit memory using atomic ions," Phys. Rev. Lett. **95**, 060502 (2005).
[6]R. G. DeVoe and C. Kurtsiefer, "Experimental study of anomalous heating and trap instabilities in a microscopic ^{137}Ba ion trap," Phys. Rev. A **65**, 063407 (2002).
[7]A. V. Steele, L. R. Churchill, P. F. Griffin, and M. S. Chapman, "Photoionization and photoelectric loading of barium ion traps," Phys. Rev. A **75**, 053404 (2007).
[8]B. Wang, J. W. Zhang, C. Gao, and L. J. Wang, "Highly efficient and isotope selective photo-ionization of barium atoms using diode laser and led light," Opt. Express **19**, 16438–16447 (2011).
[9]G. Leschhorn, T. Hasegawa, and T. Schaetz, "Efficient photo-ionization for barium ion trapping using a dipole-allowed resonant two-photon transition," Appl. Phys. B. **108**, 159–165 (2012).
[10]D. R. Leibrandt, R. J. Clark, J. Labaziewicz, P. Antohi, W. Bakr, K. R. Brown, and I. L. Chuang, "Laser ablation loading of a surface-electrode ion trap," Phys. Rev. A **76**, 055403 (2007).
[11]K. Zimmermann, M. V. Okhapkin, O. A. Herrera-Sancho, and E. Peik, "Laser ablation loading of a radiofrequency ion trap," Appl. Phys. B **107**, 883–889 (2012).
[12]H. Shao, M. Wang, M. Zeng, H. Guan, and K. Gao, "Laser ablation and two-step photo-ionization for the generation of $^{40}Ca^+$," J. Phys. Commun. **2**, 095019 (2018).
[13]G. Vrijsen, Y. Aikyo, R. F. Spivey, I. V. Inlek, and J. Kim, "Efficient isotope-selective pulsed laser ablation loading of $^{174}Yb^+$ ions in a surface electrode trap," Opt. Express **27**, 33907–33914 (2019).
[14]J. E. Christensen, "High-fidelity operation of a radioactive trapped-ion qubit, $^{133}Ba^+$," Ph.D. thesis (UCLA, Los Angeles, CA, 2020).
[15]J. Chiaverini, R. B. Blakestad, J. Britton, J. D. Jost, C. Langer, D. Leibfried, R. Ozeri, and D. J. Wineland, "Surface-electrode architecture for ion-trap quantum information processing," Quant. Inf. Comput. **5**, 419–439 (2005).
[16]K. K. Mehta, A. M. Eltony, C. D. Bruzewicz, I. L. Chuang, R. J. Ram, J. M. Sage, and J. Chiaverini, "Ion traps fabricated in a CMOS foundry," Appl. Phys. Lett. **105**, 044103 (2014).
[17]J. Stuart, R. Panock, C. Bruzewicz, J. Sedlacek, R. McConnell, I. Chuang, J. Sage, and J. Chiaverini, "Chip-integrated voltage sources for control of trapped ions," Phys. Rev. Appl. **11**, 024010 (2019).
[18]K. K. Mehta, C. Zhang, M. Malinowski, T.-L. Nguyen, M. Stadler, and J. P. Home, "Integrated optical multi-ion quantum logic," Nature **586**, 533–537 (2020).
[19]R. J. Niffenegger, J. Stuart, C. Sorace-Agaskar, D. Kharas, S. Bramhavar, C. D. Bruzewicz, W. Loh, R. T. Maxson, R. McConnell, D. Reens, G. N. West, J. M. Sage, and J. Chiaverini, "Integrated multi-wavelength control of an ion qubit," Nature **586**, 538–542 (2020).
[20]M. Ivory, W. J. Setzer, N. Karl, H. McGuinness, C. DeRose, M. Blain, D. Stick, M. Gehl, and L. P. Parazzoli, "Integrated optical addressing of a trapped ytterbium ion," Phys. Rev. X **11**, 041033 (2021).
[21]S. L. Todaro, V. B. Verma, K. C. McCormick, D. T. C. Allcock, R. P. Mirin, D. J. Wineland, S. W. Nam, A. C. Wilson, D. Leibfried, and D. H. Slichter, "State readout of a trapped ion qubit using a trap-integrated superconducting photon detector," Phys. Rev. Lett. **126**, 010501 (2021).

[22]W. J. Setzer, M. Ivory, O. Slobodyan, J. W. Van Der Wall, L. P. Parazzoli, D. Stick, M. Gehl, M. G. Blain, R. R. Kay, and H. J. McGuinness, "Fluorescence detection of a trapped ion with a monolithically integrated single-photon-counting avalanche diode," Appl. Phys. Lett. **119**, 154002 (2021).
[23]D. Reens, M. Collins, J. Ciampi, D. Kharas, B. F. Aull, K. Donlon, C. D. Bruzewicz, B. Felton, J. Stuart, R. J. Niffenegger, P. Rich, D. Braje, K. K. Ryu, J. Chiaverini, and R. McConnell, "High-fidelity ion state detection using trap-integrated avalanche photodiodes," Phys. Rev. Lett. **129**, 100502 (2022).
[24]J. M. Wilson, J. N. Tilles, R. A. Haltli, E. Ou, M. G. Blain, S. M. Clark, and M. C. Revelle, "In situ detection of RF breakdown on microfabricated surface ion traps," J. Appl. Phys. **131**, 134401 (2022).
[25]J. M. Sage, A. J. Kerman, and J. Chiaverini, "Loading of a surface-electrode ion trap from a remote, precooled source," Phys. Rev. A **86**, 013417 (2012).
[26]J. Chiaverini and J. M. Sage, "Insensitivity of the rate of ion motional heating to trap-electrode material over a large temperature range," Phys. Rev. A **89**, 012318 (2014).
[27]C. D. Bruzewicz, R. McConnell, J. Chiaverini, and J. M. Sage, "Scalable loading of a two-dimensional trapped-ion array," Nat. Commun. **7**, 13005 (2016).
[28]J. M. Stuart, "Integrated technologies and control techniques for trapped ion array architectures," Ph.D. thesis (MIT, Cambridge, MA, 2021).
[29]F. Splatt, M. Harlander, M. Brownnutt, F. Zähringer, R. Blatt, and W. Hänsel, "Deterministic reordering of $^{40}Ca^{+}$ ions in a linear segmented Paul trap," New J. Phys. **11**, 103008 (2009).
[30]M. Harlander, M. Brownnutt, W. Hänsel, and R. Blatt, "Trapped-ion probing of light-induced charging effects on dielectrics," New J. Phys. **12**, 093035 (2010).
[31]J. A. Sedlacek, J. Stuart, D. H. Slichter, C. D. Bruzewicz, R. McConnell, J. M. Sage, and J. Chiaverini, "Evidence for multiple mechanisms underlying surface electric-field noise in ion traps," Phys. Rev. A **98**, 063430 (2018).
[32]M. G. House, "Analytic model for electrostatic fields in surface-electrode ion traps," Phys. Rev. A **78**, 033402 (2008).
[33]D. J. Wineland, C. Monroe, W. M. Itano, D. Leibfried, B. E. King, and D. M. Meekhof, "Experimental issues in coherent quantum-state manipulation of trapped ions," J. Res. NIST **103**, 259–328 (1998).
[34]D. J. Berkeland, J. D. Miller, J. C. Bergquist, W. M. Itano, and D. J. Wineland, "Minimization of ion micromotion in a Paul trap," J. Appl. Phys. **83**, 5025–5033 (1998).
[35]A. H. Nizamani and W. K. Hensinger, "Optimum electrode configurations for fast ion separation in microfabricated surface ion traps," Appl. Phys. B **106**, 327–338 (2012).
[36]Y. Ibaraki, U. Tanaka, and S. Urabe, "Detection of parametric resonance of trapped ions for micromotion compensation," Appl. Phys. B **105**, 219–223 (2011).
[37]M. Fan, C. A. Holliman, X. Shi, H. Zhang, M. W. Straus, X. Li, S. W. Buechele, and A. M. Jayich, "Optical mass spectrometry of cold $RaOH^{+}$ and $RaOCH_3^{+}$," Phys. Rev. Lett. **126**, 023002 (2021).
[38]A. H. Burrell, "High fidelity readout of trapped ion qubits," Ph.D. thesis (Oxford University, Oxford, UK, 2010).